STP 1543, 2014 / available online at www.astm.org / doi: 10.1520/STP154320120215

Adrien Couet,[1] Arthur T. Motta,[2] and Robert J. Comstock[3]

Effect of Alloying Elements on Hydrogen Pickup in Zirconium Alloys

Reference

Couet, Adrien, Motta, Arthur T., and Comstock, Robert J., "Effect of Alloying Elements on Hydrogen Pickup in Zirconium Alloys," *Zirconium in the Nuclear Industry: 17th International Symposium*, STP 1543, Robert Comstock and Pierre Barberis, Eds., pp. 479–509, doi:10.1520/STP154320120215, ASTM International, West Conshohocken, PA 2014.[4]

Abstract

Although the optimization of zirconium-based alloys has led to significant improvements in hydrogen pickup and corrosion resistance, the mechanisms by which such alloy improvements occur are still not well understood. In an effort to understand such mechanisms, we conducted a systematic study of the alloy effect on hydrogen pickup, using advanced characterization techniques to rationalize precise measurements of hydrogen pickup. The hydrogen pickup fraction was accurately measured for a specially designed set of commercial and model alloys to investigate the effects of alloying elements, microstructure, and corrosion kinetics on hydrogen uptake. Two different techniques for measuring hydrogen concentrations were used: a destructive technique, vacuum hot extraction, and a non-destructive one, cold neutron prompt gamma activation analysis. The results indicate that hydrogen pickup varies not only from alloy to alloy, but also during the corrosion process for a given alloy. These variations result from the process of charge balance during the corrosion reaction, such that the pickup of hydrogen decreases when the rate of electron transport or

Manuscript received December 25, 2012; accepted for publication June 26, 2013; published online June 17, 2014.

[1]Dept. of Mechanical and Nuclear Engineering, Penn State Univ., University Park, PA 16802, United States of America (Corresponding author), e-mail: adrien.couet@gmail.com

[2]Dept. of Mechanical and Nuclear Engineering, Penn State Univ., University Park, PA 16802, United States of America.

[3]Westinghouse Electric Company LLC, Pittsburgh, PA 15235, United States of America.

[4]ASTM 17th International Symposium on *Zirconium in the Nuclear Industry* on February 3–7, 2013 in Hyderabad, India.

oxide electronic conductivity (σ_e^{ox}) through the protective oxide increases. According to this hypothesis, alloying elements (either in solid solution or in precipitates) would affect the hydrogen pickup fraction by modifying σ_e^{ox}. Because the mechanism whereby these alloying elements are incorporated into the oxide layer is critical to changing electron conductivity, the evolution of the oxidation state of two common alloying elements, Fe and Nb, when incorporated into the growing oxide layers of two commercial zirconium alloys (Zircaloy-4 and ZIRLO) and model alloys (Zr-0.4Fe-0.2Cr and Zr-2.5Nb) was investigated using x-ray absorption near-edge spectroscopy with microbeam synchrotron radiation on cross-sectional oxide samples. The results show that the oxidation of both Fe and Nb is delayed in the oxide layer relative to that of Zr, and that this oxidation delay is related to the variations of the instantaneous hydrogen pickup fraction with exposure time.

Keywords

Hydrogen pick-up, Zirconium alloys, CNPGAA, XANES, alloying elements, electronic conductivity

Introduction

As fuel burnup and reactor residence times increase, the uniform corrosion of zirconium alloy nuclear fuel cladding (and associated hydrogen pickup) can become a limiting factor for the use of high-burnup fuel rods in existing and advanced light water reactors [1,2]. Several factors can control the uniform corrosion of zirconium alloys [3]. Although alloy optimization of zirconium-based alloys used for nuclear fuel cladding has been a key to increasing corrosion resistance and reducing hydrogen pickup, a complete understanding of the role of alloying elements in the corrosion and hydrogen pickup mechanisms is still lacking.

Because very small alloying element differences cause significant differences in corrosion and hydrogen pickup, it is of interest to examine the effect of alloying elements on the corrosion and hydrogen pickup mechanisms of zirconium alloys, which can, in turn, yield significant insights potentially leading to validation of a general hypothesis on the underlying mechanisms.

The overall zirconium corrosion reaction is written as

$$Zr + 2H_2O \rightarrow ZrO_2 + 2H_2 \tag{1}$$

Some of the hydrogen generated by the corrosion reaction diffuses through the oxide and enters the metal, where it eventually can precipitate as hydrides, causing cladding embrittlement [1]. For comparison between alloys, the total hydrogen pickup fraction f_H is defined as the ratio of the hydrogen absorbed from the beginning of the corrosion test, $\Delta_0^t H_{\text{absorbed}}$, to the total amount of hydrogen that has been generated by the corrosion reaction, $\Delta_0^t H_{\text{generated}}$.

$$f_H = \frac{\Delta_0^t H_{\text{absorbed}}}{\Delta_0^t H_{\text{generated}}} \tag{2}$$

The instantaneous hydrogen pickup fraction f_H^i is defined as the ratio of the hydrogen absorbed from a time t to a time $t+\Delta t$ to the total amount of hydrogen that has been generated by the corrosion reaction during the same period.

$$f_H^i = \frac{\Delta_t^{t+\Delta t} H_{\text{absorbed}}}{\Delta_t^{t+\Delta t} H_{\text{generated}}} \tag{3}$$

Few measurements of instantaneous hydrogen pickup fractions have been reported in the literature, as they require precise hydrogen measurements at successive small exposure time intervals. The determination of f_H (and, to a lesser extent, f_H^i) on various zirconium alloys has been the subject of extensive research, but the mechanisms of hydrogen pickup and, especially, the influence of the alloy composition and microstructure on f_H are still not well understood [4–7]. Studies have shown that f_H depends strongly on alloy composition [4,6], alloy microstructure [8,9], and corrosion conditions [10]. It has been shown in the protective regime that pure Zr picks up about 20 % to 30 % of the hydrogen generated during the corrosion reaction, more than commercial alloys [11]. In general, alloying elements decrease hydrogen pickup, with the exceptions of Ni, which increases f_H, and Sn, which is reported to have no effect [11,12]. Previous measurements of instantaneous hydrogen pickup have shown that f_H^i may vary at different stages of oxide film growth [13], but no clear understanding yet exists. Some of the literature is reviewed in the following sections.

Corrosion and Hydrogen Pickup Mechanisms

RATE-LIMITING STEP IN UNIFORM ZIRCONIUM ALLOY CORROSION

The zirconium oxide formed on Zr alloys exhibits a protective character, such that after the formation of the oxide there is no direct contact between the metal and the water, and the corrosion reaction cannot happen directly, so the oxidizing species have to travel through the oxide layer. In order for zirconium oxidation to occur, either the cations or the anions have to be transported through the oxide layer. The corrosion of zirconium and its alloys in high-temperature environments occurs via oxygen anion migration through the corrosion film, with the formation of new oxide occurring at the metal–oxide interface [14,15]. The substoichiometric gradient of the zirconium oxide would be the primary driving force for the oxygen anion diffusion, although this value has not been precisely determined.

The oxidation process can be divided into several steps, as presented in **Fig. 1**. First, oxygen in the water molecule dissociates and is adsorbed onto the oxide layer surface.

$$2H_2O \xrightarrow{\text{dissociation}} 4H^+ + 2O^{2-}_{\text{adsorbed}} \tag{4}$$

FIG. 1 Schematic of the oxidation process of zirconium alloys. The chemical reactions are numbered, and the fluxes of charged species through the oxide are represented by arrows.

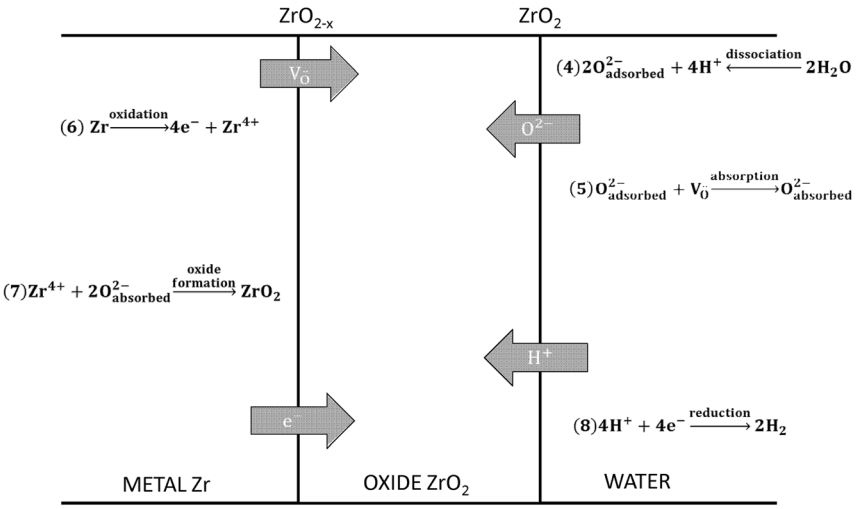

$$O^{2-}_{adsorbed} + V_{\ddot{O}} \xrightarrow{\text{absorption}} O^{2-}_{absorbed} \tag{5}$$

Because of the defect concentration gradient, the oxygen anions diffuse either through the bulk of the oxide or along the oxide grain boundaries. When the oxygen anion reaches the oxide–metal interface, it reacts with Zr cations to form new oxide.

$$Zr \xrightarrow{\text{oxidation}} Zr^{4+} + 4e^- \tag{6}$$

$$Zr^{4+} + 2O^{2-}_{absorbed} \xrightarrow{\text{oxide formation}} ZrO_2 \tag{7}$$

The formation of this new oxide releases electrons, which then migrate through the oxide to reduce the hydrogen ions at the cathodic site.

$$4H^+ + 4e^- \xrightarrow{\text{reduction}} 2H_2 \tag{8}$$

It is well known that the corrosion rate of zirconium alloys decreases as the thickness of the oxide layer increases [16]. Because of this, it is considered that either oxygen anion diffusion or electron diffusion is the rate-limiting step. This assumption leads to the parabolic scaling law for the oxidation kinetics: $\delta = Kt^n$, with $n = 0.5$ [17]. However, it has been observed that the oxidation of zirconium alloys is frequently sub-parabolic [18–21].

In the absence of externally applied potentials on the specimen, the net current through the oxide is zero, which means that the negative and positive oxidation

currents must be equal and opposite. In the case of a deviation from this balance, a potential gradient develops across the oxide thickness that equalizes these currents. If the transport of electrons through the oxide is the rate-limiting step, a positive electric gradient through the oxide layer [the potential is negative at the metal–-oxide interface relative to the oxide–water interface, $(\vec{\nabla}.V) > 0$] appears and induces a negative electric field across the oxide layer. This field slows down the diffusion of the positively charged oxygen vacancies and increases the diffusion of electrons toward the oxide–water interface through the Coulomb force $\vec{F}$ [$\vec{F} = -eZ_s(\vec{\nabla}.V)$, where $Z_{e^-} = -1$ and $Z_{V_{\ddot{O}}} = 2$]. Hence this negative electric field will tend to decrease the corrosion rate. Thus, a negative electric field tends to increase the transport of electrons and decrease the transport of oxygen vacancies. By these effects, the magnitude of the negative electric field is in turn reduced, so that the variations effected by the electric field are in a direction to decrease the rate of change in the field. Therefore, a stable situation in which the currents produce no further changes in the field is reached, and the net transport of charges at any location in the oxide is zero. Of course, the opposite is observed if the transport of oxygen vacancies is the rate-limiting step (and thus the electric field in the oxide is positive).

Many studies have observed negative potential at the metal–oxide interface relative to the oxide–water interface (the electric field in the oxide then being negative) [3,22–27]. From measurement of that potential as a function of exposure time, it also appears that electronic and ionic resistivities become more balanced as the oxide thickens, but the electric field normally remains negative. This indicates that the transport of electrons is normally slower than the transport of oxygen vacancies, making it the rate-limiting step in most circumstances. Although the mechanism of electron transport is still unclear [24,25,28,29], it seems reasonable to consider that both bulk and localized conduction can contribute to the overall rate [29–32]. The preceding arguments indicate that oxide electronic conductivity is a key parameter in controlling zirconium alloy oxidation [33,34].

Clearly, if electron transport controls the oxidation kinetics, the precipitates embedded into the growing oxide and the extrinsic compensating defects due to aliovalent cations in solid solution could have a significant effect on the corrosion kinetics by affecting the oxide electronic conductivity [35–37].

HYDROGEN PICKUP IN ZIRCONIUM ALLOYS

Hydrogen pickup in zirconium alloys has been the subject of many studies in the past 50 years, and several hydrogen pickup mechanisms have been proposed.

It has been proposed that the diffusion of hydrogen through the oxide layer would occur via solid-state diffusion through oxygen vacancies [10,38,39], with possible localized diffusion at the second phase precipitates [9]. However, the hydrogen pickup fraction would be not a function of the corrosion kinetics, but rather the result of two competing processes: hydrogen discharge (hydrogen evolution) and

the metal hydrogen uptake [5,40], with the alloying elements embedded in the oxide layer affecting both of these processes.

It is well accepted in the literature that Nb has a beneficial effect on hydrogen pickup, significantly decreasing the hydrogen pickup fraction [41–43]. This can be explained by the doping effect of the donor Nb^{5+} at the interface with the aqueous medium, which increases the electron concentration at the oxide–water interface, thereby promoting the hydrogen discharge process [26,44]. Electrochemical measurements have also shown that oxide electronic conductivity is increased by Nb additions, promoting hydrogen evolution at the oxide–water interface and reducing hydrogen uptake [34]. However, these effects cannot readily explain the observed variations of f_H^i as a function of exposure time [13]. The effect of the addition of transition metals such as Ni, Fe, and Cr on hydrogen pickup has also been studied, and it has been shown that for a given oxide thickness, Zircaloy-2 absorbs more hydrogen than Zircaloy-4. Also, the conclusion has been drawn that Ni has a detrimental effect on hydrogen pickup [4,8,45]. The effect of second-phase precipitates on hydrogen pickup is, however, still unclear [7], with different results depending on the precipitate size and distribution [9,33].

OBJECTIVE OF THE STUDY

The foregoing illustrates the need to understand the effects of alloying elements on hydrogen pickup so as to design better alloys. In order to contribute to this understanding, we used a non-destructive technique called cold neutron prompt gamma activation analysis (CNPGAA) to quantitatively assess hydrogen concentrations in zirconium alloys. Using this nondestructive technique coupled with a conventional vacuum hot extraction (VHE) technique, we systematically measured the hydrogen pickup fraction at different exposure times for a set of zirconium alloys with specific chemistries and microstructures. The evolution of the chemical states of two alloying elements, Fe and Nb, when incorporated into the oxide layers formed during autoclave testing of various zirconium alloys was examined using micro x-ray absorption near-edge spectroscopy (μXANES).

Experimental Procedures

ALLOYS

The alloys used in this study are listed in **Table 1** and included production materials Zircaloy-4 and ZIRLO and model alloys Zr-2.5Nb, pure sponge Zr, and Zr-0.4Fe-0.2Cr. All alloys were in the recrystallized state except for Zircaloy-4 tube, which was in a cold work stress relieved state. The starting hydrogen concentration in the alloys prior to autoclave testing was 10 to 15 wt. ppm.

The zirconium alloy samples were in the form of corrosion sheet coupons (25 mm by 20 mm by 0.8 mm) or tubing as shown in **Table 1**. The alloys were processed following a procedure described in Ref 46. Two of the alloys were processed at 580°C, to minimize grain growth for pure zirconium (sponge) and to maintain small precipitates in the Zr-0.4Fe-0.2Cr (L) alloy. A high process temperature of

TABLE 1 Description of the chemical composition and geometry of the commercial and model alloys used in this study. (L) and (H) denote small and large precipitate size, respectively (see text) [21].

	Alloy System	Alloy Composition, wt. %	Sample Geometry
Model alloy	Pure Zr	Zr sponge	Sheet
	Zr–Fe–Cr	Zr-0.4Fe-0.2Cr (L)	Sheet
		Zr-0.4Fe-0.2Cr (H)	
	Zr–Nb	Zr-2.5Nb	Tube
Commercial alloy	ZIRLO	Zr-1.0Nb-1.0Sn-0.1Fe	Sheet and tube
	Zircaloy-4	Zr-1.45Sn-0.2Fe-0.1Cr	Sheet and tube

720°C was used to grow large precipitates in the Zr-Fe-Cr (H) alloy. The average precipitate diameter determined via synchrotron diffraction in Zr-0.4Fe-0.2Cr (L) and Zr-0.4Fe-0.2Cr (H) is equal to 40 nm and 110 nm, respectively [47].

CORROSION TEST

Corrosion tests were performed at Westinghouse Electric Co. autoclave facilities in Churchill, PA. The samples were corroded in 360°C pure water in saturated pressure conditions at 18.7 MPa (2708.6 psi) according to ASTM G2 [48]. After every exposure cycle, the autoclave was opened and the water was refreshed in order to maintain a low hydrogen concentration in the water. In addition, all samples were weighed at the end of each cycle to measure weight gain as a function of exposure time. Sister samples from each alloy were periodically archived for subsequent destructive measurement of hydrogen content. Some selected samples were used for the nondestructive measurement of hydrogen content via CNPGAA. After hydrogen content measurements, these samples were returned to the autoclave for additional exposure, followed by further CNPGAA measurements of hydrogen concentrations, so that the evolution of the hydrogen pickup fraction was characterized on single samples.

HYDROGEN MEASUREMENTS

The hydrogen pickup fraction was determined at different exposure times using a combination of two different techniques, VHE and CNPGAA, described in the following paragraphs.

VHE was performed by LUVAK, Inc. (Boylston, MA). An NRC Model 917 apparatus [49] was used for VHE. The technique is described in detail elsewhere [50].

Because the technique is destructive, it is necessary to perform several measurements on different samples (sister samples), which is intrinsically a cause of measurement dispersion. Also, the experimental error is not well characterized, and the average experimental error is approximately ±5 %, as confirmed by different studies [13,51]. The dimensions of the analyzed samples were 8 mm by 8 mm for sheet

coupons and a 3-mm-long ring in the case of tubes. In most cases, several samples from the same coupons were analyzed to improve the accuracy of the results.

The procedure for CNPGAA measurements in zirconium alloys is discussed in detail elsewhere [50]. CNPGAA on ZIRLO and Zircaloy-4 sheet samples was performed at the National Institute of Standards and Technology (NIST) (Gaithersburg, MD) in one of the cold neutron beam lines. The background noise at the hydrogen gamma ray energy at this beamline is extremely low, so concentrations as low as 5 wt. ppm of hydrogen in zirconium alloys are detectable.

HYDROGEN PICKUP FRACTION

The hydrogen pickup fraction of a sample was calculated from the measurement of its weight gain and its hydrogen content. The calculation assumed no loss of oxide during corrosion. This assumption was verified by the good correspondence between weight gain and oxide layer thickness measured using scanning electron microscopy (SEM) on polished cross-sections of the corrosion sample. In addition, the weight gain was assumed to be due only to oxygen and to not take into account the hydrogen uptake. This is a good assumption for low hydrogen pickup fractions, but one has to keep in mind that the hydrogen uptake resulting from a theoretical hydrogen pickup fraction of 100 % could account for 11.1 % of the total weight gain. Because the autoclave is opened at least every 30 days, no significant build-up of hydrogen gas is observed (during the early stages of corrosion, in which corrosion rates are higher and thus hydrogen gas releases are more significant, the autoclave was opened more often).

Following these assumptions, f_H is equal to [46]

$$f_H = \frac{10^{-6}(m_s^t C_H^t - m_s^i C_H^i)}{2\dfrac{(m_s^t - m_s^i)}{M_O} M_H} \tag{9}$$

where:

m_s^t = mass of the sample at the time of the measurement,
m_s^i = mass of the bare sample,
M_O = atomic mass of the oxygen atom,
M_H = atomic mass of the hydrogen atom,
C_H^i = initial concentration of hydrogen in the sample, wt. ppm, and
C_H^t = concentration of hydrogen at the time of measurement, wt. ppm.

The instantaneous pickup fraction f_H^i is given by

$$f_H^i = \frac{10^{-6}(m_s^{t+\Delta t} C_H^{t+\Delta t} - m_s^t C_H^t)}{2\dfrac{(m_s^{t+\Delta t} - m_s^t)}{M_O} M_H} \tag{10}$$

The hydrogen pickup fraction errors originating from weight gain and hydrogen concentration measurements have been evaluated using an error propagation formula.

X-RAY ABSORPTION NEAR-EDGE SPECTROSCOPY EXPERIMENT

Micro-XANES experiments were performed at the 2ID-D beamline of the Advanced Photon Source (APS) at Argonne National Laboratory [52]. **Figure 2** shows a schematic of the scattering and data-acquisition geometry for the XANES experiments: a focused synchrotron microbeam (0.2 μm in diameter) is placed in frontal incidence on the region of interest of the cross-sectional oxide specimen. The XANES signals are recorded in fluorescence. The XANES scan energy step is 0.5 eV, and the chosen energy windows are 100 eV (from 7.09 keV to 7.19 keV) for Fe (the Fe K-edge is located at 7.12 keV) and 140 eV (from 18.94 keV to 19.08 keV) for Nb (the Nb K-edge is located at 18.98 keV). All measurements were performed at room temperature.

The experimental procedure consisted of first recording a fluorescence scan of the oxide layer Zr L-edge (in case of Fe) or Zr K-edge (in case of Nb) to determine the positions of the oxide–metal and oxide–water interfaces. XANES scans were performed at various distances from the metal–oxide interface, both in the oxide and in the metal. In order to rule out specimen drift during the experiment, after each XANES scan an extra fluorescence scan was obtained to confirm the oxide position.

A list of the corrosion samples that were archived and used in the XANES experiments with the exact exposure time and oxide thickness (determined from weight gains) is shown in **Table 2**.

In order to determine the chemical state of Fe and Nb in the zirconium oxide layer, Fe K-edge and Nb K-edge XANES spectra of reference standards were measured. The processing of XANES spectra was performed using Athena software (version 0.8.061, Ifeffit 1.2.11c) [53].

FIG. 2 Schematic drawing showing the geometry of data acquisition at the synchrotron beamline.

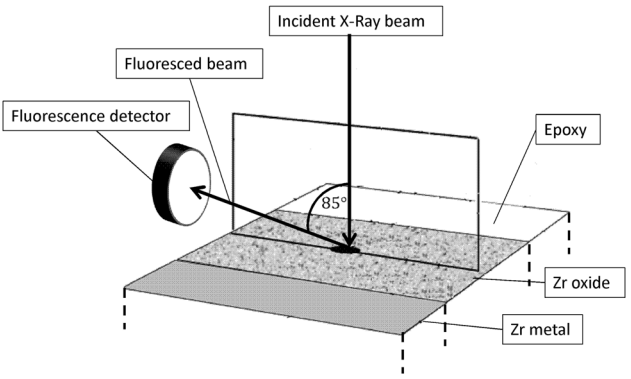

TABLE 2 List of the samples used for the XANES experiments. Their exposure time (in days) and their oxide thickness (in micrometers, derived from the weight gain) are indicated.

			Exposure Time, days	Oxide Thickness, μm
Fe	Zircaloy-4	Before first transition	45	1.7
			60	1.9
		Between first and second transitions	90	2.8
			105	3.4
			120	3.6
			135	3.9
			150	4.1
			165	4.2
		Between second and third transitions	225	5.9
			255	6.4
	Zr-0.4Fe-0.2Cr(H)	Pre-breakaway	173	2.4
			463	3.2
	ZIRLO	Before first transition	30	1.7
			60	2.3
			90	2.7
Nb	ZIRLO	Before first transition	30	1.7
			60	2.3
			90	2.7
		Between first and second transitions	240	5.5
	Zr-2.5Nb	Before first transition	60	1.7
			120	2.7
			150	3.2

The different Fe and Nb standards used for the XANES experiments are detailed at length elsewhere [52], and the list is presented in **Table 3**.

The oxide samples were in the form of small transverse cross-sections (the transverse direction being normal to the cross-section) of corroded sheet coupons prepared according to a procedure detailed elsewhere [52].

A schematic drawing of the final sample configuration is shown in **Fig. 3**. The sample thickness was approximately 200 μm. The incident beam being parallel to the transverse direction, the measured XANES signal as a function of distance from the oxide–metal interface includes contributions from the alloying element (Fe or Nb) both in precipitates and in solid solution, as the x-ray attenuation length is approximately 12.5 μm at 7.12 keV and 28 μm at 18.98 keV [54], which results in a sampled volume that is tens of micrometers deep.

For Zircaloy-4, assuming that the ratios of Fe and Cr in the precipitates and in the alloy are the same (which has been found to be true for $\mathrm{Fe(wt.\ \%)/Cr(wt.\ \%)} < 4$

TABLE 3 List of the different standards used in the fitting process for XANES spectra [52].

	Alloy	Metal Standard [52]	Oxide Standard
Fe	Zircaloy-4	Fe bcc	Fe_2O_3 powder
		Fe in Zircaloy-4 metal	Fe_3O_4 powder
	Zr-0.4Fe-0.2Cr	Fe in $Zr(Fe,Cr)_2$ SPP	FeO powder
		Fe in pure Zr	
	ZIRLO	Fe bcc	Fe_2O_3 powder
		Fe in ZIRLO metal	Fe_3O_4 powder
		Fe in pure Zr	FeO powder
Nb	ZIRLO	Nb powder	NbO powder
		Nb in ZIRLO metal	NbO_2 powder
			Nb_2O_5 powder
	Zr-2.5Nb	Nb powder	NbO powder
		Nb in Zr-2.5Nb metal	NbO_2 powder
			Nb_2O_5 powder

[55]) and the concentration of Fe in solid solution ranges between 50 and 200 wt. ppm [56], the volume fraction of precipitates is approximately 0.5 %, and the total amount of Fe in second-phase precipitates is approximately 10 to 40 times the amount of Fe in solid solution. Although the fluorescence signal is not directly proportional to the concentration, we can conclude that the contribution of alloying elements in solid solution

FIG. 3 Schematic drawing showing the geometry of the samples used for XANES in a transverse cross-section top view.

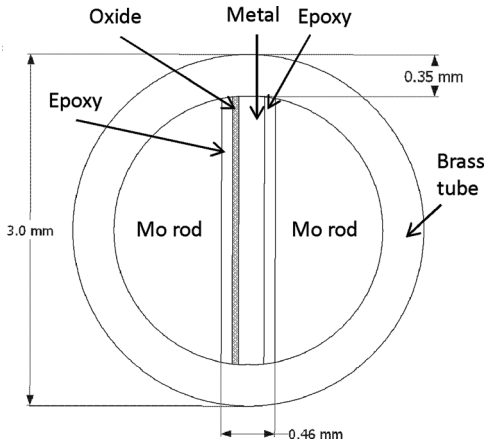

in the XANES signal coming out from the bulk samples cannot be neglected. The probability that the x-ray beam will hit a single precipitate as a function of oxide depth in our samples as calculated in Ref 52 is equal to 100 % for samples as thick as 200 μm. Thus the recorded XANES spectra are a convolution of signals from Fe in both solid solution and precipitates, so that the deconvolution of Fe signals from solid solution and precipitates during the processing of XANES spectra is impossible.

Results

CORROSION TEST

The corrosion weight gains for the different alloys as a function of exposure time are plotted in **Fig. 4**. The plotted weight gains represent an average of the whole set of sister samples. The standard deviations of weight gain measurements among sister samples of a given alloy at a given exposure time are less than 0.5 mg/dm^2. The samples indicated by arrows have been archived and used for XANES experiments. The commercial alloys show the well-defined transition-type corrosion behavior that has been observed previously in Zr alloys [20]. The oxide thicknesses at the first transition are 2.1 μm for Zircaloy-4, 2.9 μm for ZIRLO, and 3.5 μm for Zr-2.5Nb (1 μm = 14.77 mg/dm^2).

The Zr–Fe–Cr model alloys did not show a transition up to a corrosion time of 463 days. The corrosion data of pure Zr are not shown after 14 days because the alloy underwent a sudden breakaway and loss of protectiveness, as confirmed by SEM characterizations of the oxide layers, which also showed lateral and longitudinal cracks and significant preferential oxide growth in the zirconium metal (in the form of dendrites).

TOTAL HYDROGEN PICKUP FRACTION

The hydrogen contents (mg/dm^2) of zirconium alloys as a function of weight gain (mg/dm^2) are plotted in **Figs. 5** and **6**. The dashed lines represent the hydrogen content as a function of weight gain for constant f_H of 10 %, 20 %, and 30 %. The hydrogen contents measured via CNPGAA are marked by a star on the expanded view of **Fig. 5**. At a given weight gain wide variations are seen in f_H between alloys. Additionally for a given alloy, f_H significantly changes (increases) with oxide thickness for a given alloy.

Figure 5 shows that the total hydrogen pickup fraction of pure Zr before breakaway is equal to 18 %, whereas that for Zircaloy-4 in the pre-transition regime is lower than 10 %, suggesting that the presence of precipitates reduces hydrogen pickup, as Sn is known to have almost no effect on hydrogen pickup [4,6]. This is confirmed by the pickup fraction of approximately 10 % measured for the model alloy ZrFeCr for the same oxide thickness (see **Fig. 6**). The f_H of ZIRLO is consistently lower than that of Zircaloy-4, whereas the f_H of Zr-2.5Nb at a given oxide thickness is the lowest of the samples measured, which suggests that the addition of Nb decreases the hydrogen pickup fraction.

FIG. 4 Weight gain as a function of exposure time for the following alloys: (a) ZIRLO sheet; (b) Zircaloy-4 sheet; (c) Zr-2.5Nb; (d) pure sponge zirconium; (e) Zr-0.4Fe-0.2Cr (L); and (f) Zr-0.4Fe-0.2Cr (H). The arrows indicate the samples that were archived and studied using XANES.

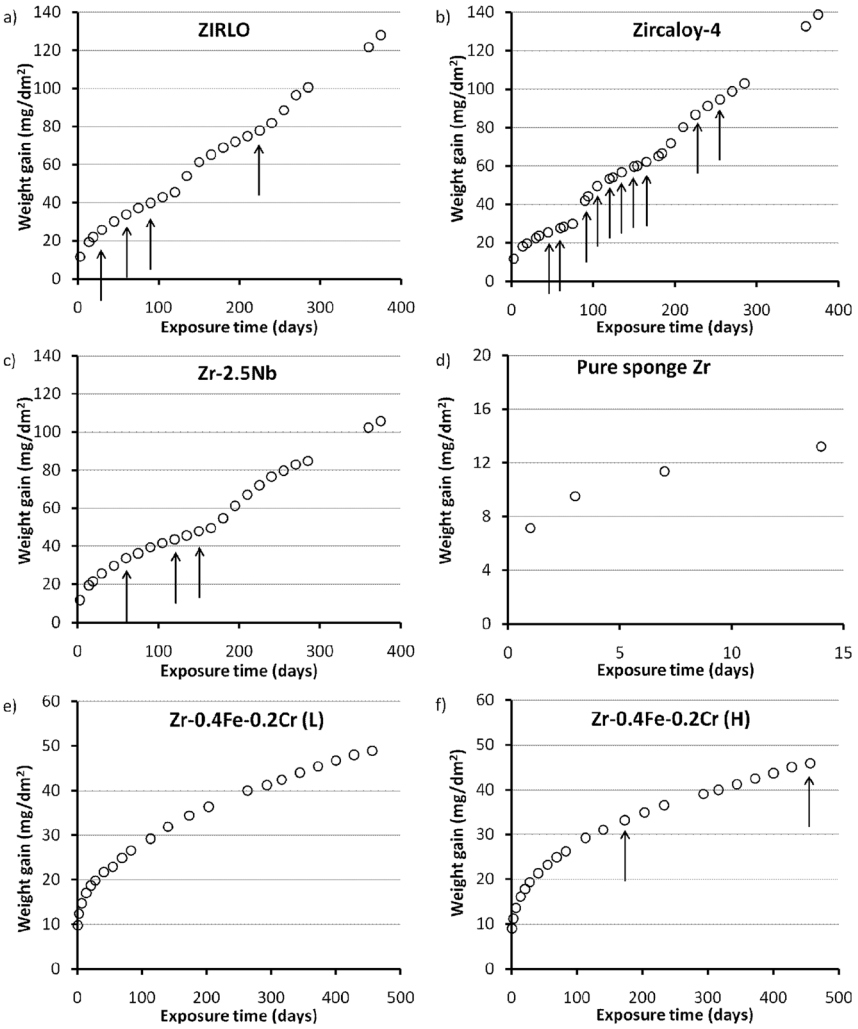

It is apparent from Figs. 5 and 6 that for all the alloys studied, the overall f_H varied significantly with oxide thickness. One point to note is that the f_H was higher for the weight gain acquired between the first and second transitions than before the first transition, and still higher between the second and third transitions. This is in spite of considerable evidence that the corrosion kinetics are repetitive and the oxide layer reforms itself in each transition. This suggests that the presence of the

FIG. 5 Hydrogen content as a function of weight gain (and oxide thickness) for the alloys studied. The corrosion data are available in Fig. 4. The dashed lines correspond to constant total hydrogen pickup fractions of 10 %, 20 %, 30 %, and 40 %. An expanded view of early exposure time is also displayed. Hydrogen contents of samples marked by a star have been measured via CNPGAA.

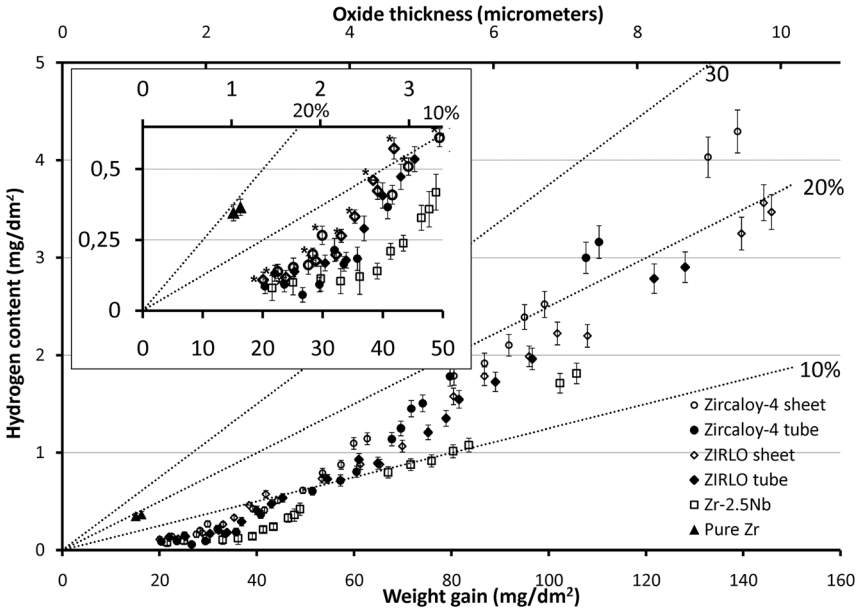

porous oxide formed during previous transitions might act to increase hydrogen pickup although this oxide is permeable to water.

At the end of the corrosion test, after 375 days of corrosion, f_H was equal to 25 % for Zircaloy-4 and 19 % for ZIRLO.

The value of f_H increased significantly from the pre-transition period to the first transition period (the transitions are marked by a sudden increase in weight gain, as seen in **Fig. 4**; the first transition period is defined as the period between the first and second transitions) and, to a lesser extent, from the first transition period to the second transition period. It also appears that f_H varied within the transition periods, which would suggest that there are significant variations of f_H^i even though the corrosion kinetics changes only smoothly (see **Fig. 4**). This particular point is discussed in more detail in the next section.

The value of f_H also depends on the alloy microstructure. The hydrogen content as a function of weight gain is plotted for the two Zr–Fe–Cr model alloys in **Fig. 6**. Before reaching a thickness of approximately 3 μm, both alloys have similar f_H values (between 10 % and 15 %). After the oxide thickness reached 3 μm, we observed an increase in f_H, whereas the corrosion kinetics remained unchanged (see **Fig. 4**).

FIG. 6 Hydrogen content as a function of weight gain (and oxide thickness) for the alloys Zr-0.4Fe-0.2Cr (L) and Zr-0.4Fe-0.2Cr (H). The corrosion data are available in Fig. 4. The dashed lines correspond to constant total hydrogen pickup fractions of 10 %, 20 %, and 30 %. The hydrogen content of the sample marked by a star has been measured via CNPGAA.

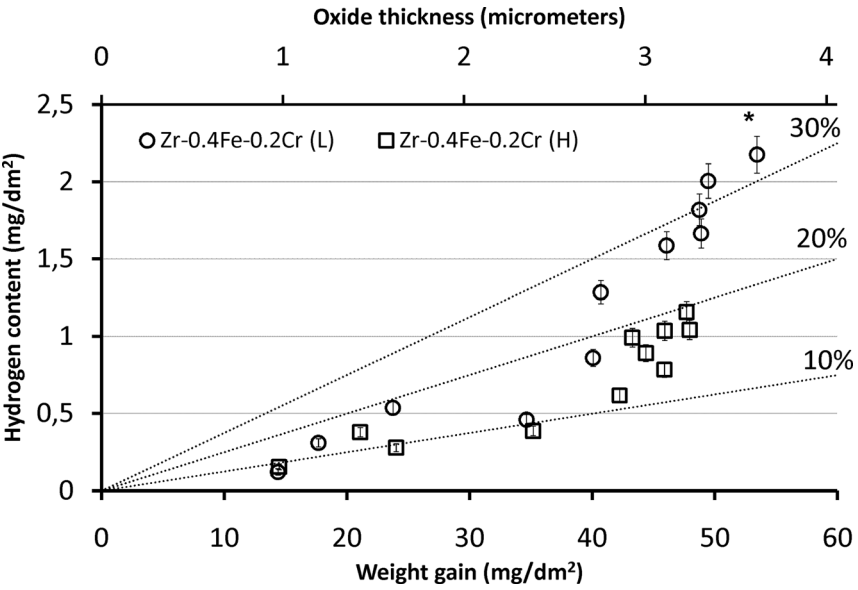

Even though both model alloys show that f_H increased once the oxide was approximately 3 μm thick, the alloy with bigger precipitates was less sensitive to that increase. This suggests that for a given volume fraction and corrosion rate, alloys with bigger $Zr(Fe,Cr)_2$ precipitates tend to pick up less hydrogen than alloys with smaller precipitates.

As discussed in the preceding section, the zirconium alloys' oxidation kinetics follow a power law of the form Kt^n. We determined the exponent n by fitting the weight gain curves by a power law. The R^2 of the power law fitting was kept above 0.999 to ensure a good fit. The total hydrogen pickup fraction at the last fitted point (approximately 50 days of exposure time) is plotted in Fig. 7 as a function of the exponent n. An inverse relationship between the corrosion kinetics and f_H is observed: the lower the value of n, the greater the value of f_H. Relative to pure Zr, the addition of $Zr(Fe,Cr)_2$ precipitates tends to increase the kinetics and lower the f_H. Nb-containing alloys have the fastest corrosion kinetics but the lowest hydrogen pickup. Even though they are not discussed in this paper, we also added Zr-0.5Cu and Zr-2.5Nb-0.5Cu alloys to this plot. It appears that relative to pure Zr, the addition of Cu slows down the kinetics but increases the hydrogen pickup fraction.

FIG. 7 Total hydrogen pickup fraction at the last fitted point (generally 50 days of exposure) as a function of the exponent n from the power law fit of the weight gain $w_g = kt^n$ for various zirconium alloys.

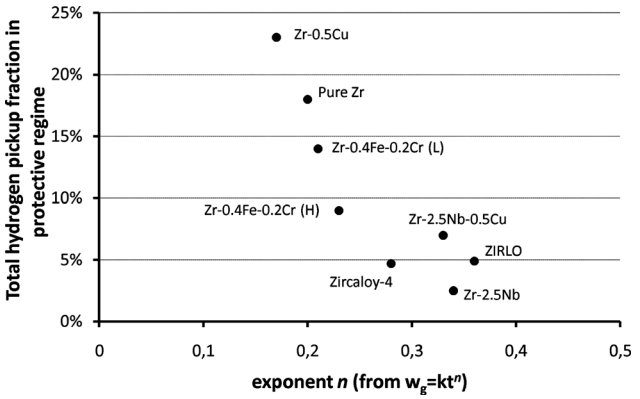

INSTANTANEOUS HYDROGEN PICKUP FRACTION

We calculated the instantaneous hydrogen pickup fraction of commercial alloys in order to better characterize the evolution of hydrogen pickup as a function of corrosion kinetics. The results are presented in **Fig. 8** for the ZIRLO sheet. All results came from VHE measurements on sister samples. The weight gains of the samples that were analyzed for hydrogen are also indicated in the figures. Two plots of f_H^i are superimposed in the figures because half of the sister samples in the autoclave had 15 more days of corrosion than the other half. Thus, with the autoclave being opened every 30 days, half of the samples had a corrosion time of t and the other half had a corrosion time of $t + 15$ days. Two f_H^i curves are plotted, one for each set of sister samples. The time Δt between two measurements of f_H^i was generally equal to 30 days.

The f_H^i error bars are rather large because of the small Δt and the errors from the VHE measurements, which led to more uncertainties, especially when the corrosion rate was low. However, a general trend is observed in these plots. Similar trends have been observed for Zircaloy-4, Zr-2.5Nb-0.5Cu, and Zr-2.5Nb alloys [46]. It is clear that f_H^i varies as a function of exposure time. At first, when the corrosion rate is high, f_H^i is low (around 5 % in the pre-transition regime). As the exposure time increases, the corrosion rate slows down and f_H^i increases significantly. The instantaneous hydrogen pickup fraction keeps on increasing until the sample reaches transition. At transition, the corrosion rate increases again, and f_H^i drops. The process then repeats itself in the second transition regime, and so on, following the periodicity of corrosion kinetics. The instantaneous hydrogen pickup fraction evolution has been confirmed by following the pickup fraction of a given sample using CNPGAA to measure its hydrogen content at regular time intervals [46], so

FIG. 8 Instantaneous hydrogen pickup fraction and weight gain as a function of exposure time (in days) for ZIRLO sheet alloy.

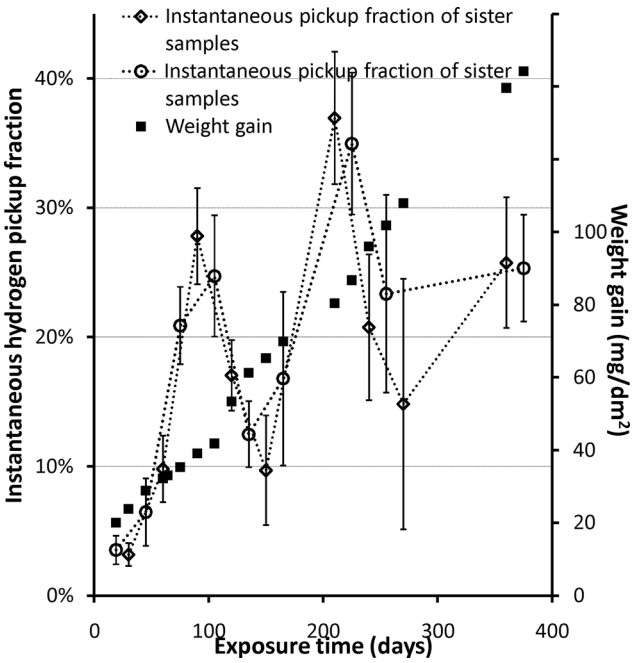

that the dispersion of results due to sister sample variations and spot-to-spot variations are minimized.

After the first transition, f_H^i decreases to approximately 10 % to 15 %, and not to the 5 % observed at the beginning of corrosion. Similarly, f_H^i at the second transition reaches higher values than at the first transition. These increases in f_H^i from one transition period to another lead to the observed increases in f_H in Fig. 5.

FE AND NB OXIDATION STATES

To quantify the Fe and Nb chemical states as measured by μXANES, the spectra were fit using the linear combination fitting algorithm included in the Athena software [53] (in this case, 14 spectra were used, including Fe_2O_3, Fe_3O_4, bcc-Fe, FeO, Fe in Zr, etc. [see Table 3]). Through the fitting, we quantified the fraction of alloying element that had been oxidized in the oxide. In all alloys, the fractions of oxidized Fe and Nb were close to zero at the metal– oxide interface and gradually increased in the protective oxide (the oxide formed since the previous transition), finally reaching 100 % some distance from the oxide–metal interface, indicating that all of the Fe and Nb was oxidized in the outer part of the oxide. The oxidation of Fe and Nb (both in precipitate and in solid solution) is delayed relative to the

oxidation of Zr, so that a significant fraction of Fe and Nb remains metallic in the oxide layer, as already observed [57,58].

To compare the evolution of alloying element oxidation states between samples of different oxide thicknesses (i.e., at different exposure times), we chose the parameter δ_{met}, defined as the length of the oxide layer in which the fraction of metallic Fe or Nb is above 50 %. Thus δ_{met} is an indication of the evolution of the oxygen potential in the oxide layer. We also define δ_p as the protective oxide thickness (defined as the oxide formed since the previous transition). The ratio δ_{met}/δ_p is an indicator of the fraction of the oxide in which alloying elements are mainly unoxidized. Values of δ_{met} for Fe in Zircaloy-4 and ZIRLO and for Nb in ZIRLO and Zr-2.5Nb as a function of δ_p are shown in Fig. 9. The transition thickness is represented by the shaded area. Because there are some variations in transition thickness from one transition period to another, the transition thickness is represented by a shaded area for ZIRLO and Zircaloy-4 in Fig. 9, and not by a straight line. Also, because the

FIG. 9 δ_{met} (in microns) as a function of the protective oxide thickness δ_p (in microns) for (a) Fe in Zircaloy-4 sheet, (b) Fe and Nb in ZIRLO tube, (c) Nb in Zr-2.5Nb, and (d) Fe in Zr-0.4Fe-0.2Cr (H). The shaded area shows the transition thickness for the different alloys.

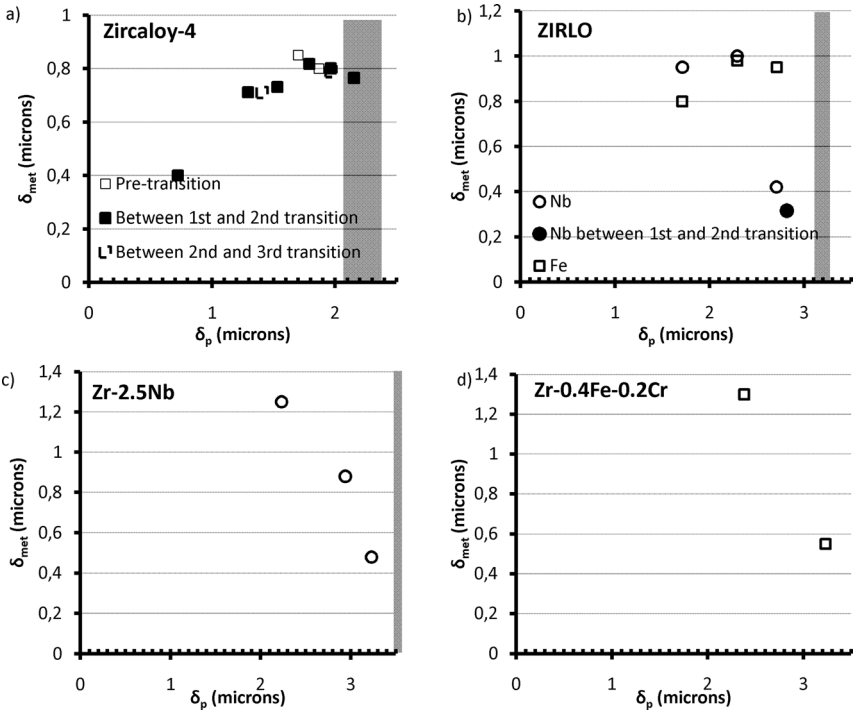

oxide thickness increases rapidly right after transition, it is difficult to archive a sample with small δ_p; hence the lack of data at small values of δ_p.

Generally, at first, δ_{met} increases up to a threshold value of approximately 0.8 μm for Zircaloy-4, 1 μm for ZIRLO, and 1.2 μm for Zr-2.5Nb. The threshold value for the model alloy Zr-0.4Fe-0.2Cr (H) is at least 1.25 μm. Once δ_{met} reaches its threshold value, it remains constant up to the time when the oxide reaches its transition thickness. At the transition, it is believed that δ_{met} drops, to zero. Interestingly, between the points at δ_p equal to 2.4 μm and δ_p equal to 3.2 μm for Zr-0.4Fe-0.2Cr (H), we observed a decrease in δ_{met} suggesting that although the corrosion kinetics do not change, a loss of protectiveness might be imminent.

As expected, δ_{met} does not depend on the transition period (see the results for Zircaloy-4 and ZIRLO), as it is directly dependent on the oxygen potential in the oxide layer and it is known that the corrosion of Zircaloy-4 is periodic [20]. Thus the evolution of the oxidation of alloying elements is periodic from one transition period to another.

Discussion

The results above indicate that hydrogen pickup results from the need to balance charge such that when oxide electronic conductivity (σ_e^{ox}) decreases, a driving force exists for hydrogen ingress.

RELATIONSHIP BETWEEN OXIDATION KINETICS AND HYDROGEN PICKUP FRACTION

As discussed previously, different alloys have different oxidation kinetics, with Nb alloys being closer to parabolic, whereas pure Zr and Fe/Cr-based alloys are subcubic. Similar variations in the oxidation kinetics of zirconium binary alloys have already been noticed [19]. If we assume that the electron transport is rate limiting, the hydrogen pickup mechanism will be linked to the corrosion kinetics through the electron flux: the higher the oxide electronic conductivity, the higher the electron flux (and thus the higher the corrosion rate) and the lower the hydrogen pickup fraction. This is also in accordance with results reported on binary Zr–Fe alloys [59] and on Zr–Sn–Fe–Cr alloys [60].

Striking and consistent variations in f_H^i were observed in this work, with f_H^i increasing consistently before transition, dropping at transition, and increasing in the following transition period, in agreement with previous results [13]. One of the possible hypothesis for the variations of f_H^i could be that the hydrogen pickup fraction is only a phenomenological characteristic and that the rate of hydrogen picked up by the metal is actually constant, so that f_H appears higher at lower corrosion rates. Using CNPGAA on given samples to measure the quantity of hydrogen picked up by the metal as a function of exposure time, it is possible to show that the actual quantity of hydrogen picked up varies as a function of exposure time, which negates this hypothesis [46]. The present results show that the hydrogen pickup

fraction is linked to the corrosion kinetics, although it does not follow this kinetics. A likely explanation is that initially the corrosion rate is high, because electron transport is easy. When the evolution of alloying elements in the oxide layers for example by oxidation of precipitates causes the electronic conductivity to decrease, the corrosion rate decreases, and concomitantly, a driving force is established that enhances hydrogen ingress. Thus alloying elements are a key parameter of the hydrogen pickup mechanism, in agreement with the fact that f_H changes from alloy to alloy. Their effect on hydrogen pickup is discussed in the next sections in terms of the effect of Nb and the effect of precipitates.

Effect of Nb Addition on f_H

Nb additions decrease the hydrogen pickup fraction. Kiselev et al. studied the effect of Nb additions on f_H in binary Zr–Nb alloys [41] and concluded that as the Nb concentration increases, the corrosion rate and therefore the amount of hydrogen produced increase, but the hydrogen pickup fraction decreases, especially in the solid solution range (up to 0.5 wt. % [61]). In our study, we also observed that Zr-2.5Nb alloy showed both the lowest f_H^t throughout the experiment and the highest corrosion rate. The presence of Nb^{5+} in the oxide is indicated by the fact that the Nb XANES spectra showed absorption edges above the Nb^{4+} edge, although it is possible that a contribution of lower valences also exists [58,62]. The presence of the Nb_2O_5 phase in Zr-2.5Nb oxides has also been confirmed by photoelectrical analysis of passive zirconium niobium oxide layers [63]. Oxidized Nb atoms dissolved in the ZrO_2 solid solution would dope the oxide layer and act mostly as donors. If we do not consider the aggregation of alloying elements and the formation of complex defects, the compensating defect of the Nb positive charge will be either zirconium vacancies or electrons. Given that the conduction band of ZrO_2 is formed of zirconium 3*d* empty states and the zirconium vacancy is highly positively charged, it is believed that electrons are the preferred compensating defects.

According to this picture the oxide electronic conductivity would increase as a result of the increase in the free electron concentration. This result is also confirmed by electrochemical measurements on zirconium alloys, with Zr-2.5Nb showing by far a lower electronic resistance than other Zr alloys [33]. As a result it is believed that an increase in oxide electronic conductivity would reduce the hydrogen pickup fraction. As it is believed that electron transport is the rate-limiting step in zirconium alloy oxidation (see the section "Rate-limiting Step in Uniform Zirconium Alloy Corrosion"), the increase in oxide electronic conductivity could also explain the faster kinetics observed in Zr–Nb alloys, which is closer to parabolic than cubic. This hypothesis could also explain why the size and volume fraction of Nb precipitates do not play a significant role in determining the hydrogen pickup fraction and corrosion resistance of Zr–Nb alloys, as the dominant effect would be a low electronic resistivity due to the donor effect of Nb in solid solution.

Effect of Precipitates on f_H

The presence of $Zr(Fe,Cr)_2$ precipitates appears to reduce the hydrogen pickup fraction relative to pure Zr. In agreement with previous observations, the μXANES results show that precipitates remain metallic when embedded in the growing zirconium oxide layer up to a certain distance from the metal–oxide interface. Metallic precipitates would likely enhance the electronic conductivity of the oxide layer, which would in turn reduce the hydrogen pickup relative to pure Zr. It is believed that a material with a homogeneous distribution of fine precipitates has a higher oxide electronic conductivity than pure Zr [34,37].

For a given volume fraction and corrosion rate, the f_H of the alloy with larger $Zr(Fe,Cr)_2$ precipitates is lower than the f_H of the alloy with smaller $Zr(Fe,Cr)_2$ precipitates. Electrochemical measurements have shown that for a given volume fraction, Zircaloy-4, with bigger $Zr(Fe,Cr)_2$ precipitates, would have a greater oxide electronic conductivity than alloys with smaller precipitates [33], resulting in a lower f_H. Metallic precipitates can act as local electric shortcuts favoring electronic conduction, thus promoting hydrogen evolution at the oxide–water interface and resulting in a low hydrogen pickup fraction. However, μXANES results have shown that precipitates do not remain metallic and oxidize after a certain distance from the oxide– metal interface, so that they could not act as local electric shortcuts throughout the oxide layer.

Precipitate oxidation and its effect on hydrogen pickup fraction are the subject of the next sections.

Oxidation Model of Precipitates

The μXANES measurements in Zircaloy-4, ZIRLO, Zr-2.5Nb, and Zr-0.4Fe-0.2Cr alloys reported in this work [64,65] show that the oxidation of Fe and Nb in precipitates is delayed relative to the oxidation of Zr. This is in accordance with previous transmission electron microscopy observations [65] and electrochemical measurements [66]. Zirconium is preferentially oxidized and alloying elements in precipitates are protected up to a certain distance from the oxide–metal interface where the oxygen potential is high enough to oxidize Fe or Nb in precipitates. As reported in the literature, first Cr is oxidized and metallic Fe segregates to form bcc Fe [52]. In general, once the oxidation potential of alloying elements in precipitates is reached, they start oxidizing.

The oxidation model based on the μXANES results proposed in Ref 52 is recalled here. Right after the oxide transition, the oxide layer is fully protective and a continuous oxygen potential gradient across the oxide layer is established. The boundary conditions at the interfaces fix the oxygen potentials at these locations. As δ_p increases, the oxygen potential gradient decreases, so that δ_{met} also increases, but the ratio δ_{met}/δ_p remains constant [see **Fig. 10(*a*)**]. As δ_p continues to increase, δ_{met} reaches a threshold value and remains constant. Thus, the ratio δ_{met}/δ_p decreases and the oxygen potential in the outer part of the protective oxide increases [see **Fig. 10(*b*)**]. The threshold value of δ_{met} depends on the alloy and is

FIG. 10 Schematic evolution of the oxidation of precipitates in the zirconium oxide layer as a function of the oxygen partial pressure across the oxide: (a) before δ_{met} reached its threshold value; (b) after δ_{met} reached its threshold value.

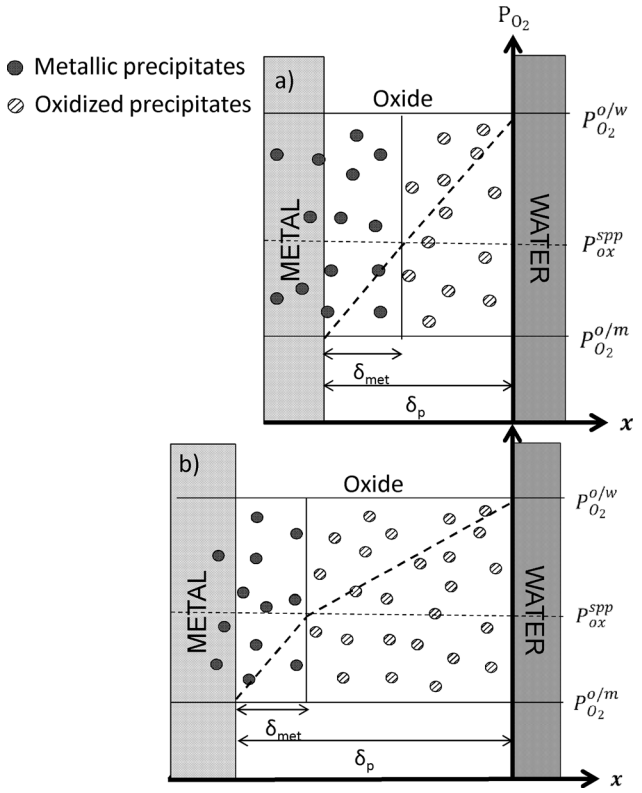

smaller for Zircaloy-4 (∼800 nm) than for ZIRLO (∼1.0 μm), and the value for ZIRLO is smaller than δ_{met} in Zr-2.5Nb (∼1.2 μm) and Zr-0.4Fe-0.2Cr (H) alloy (at least 1.25 μm). The oxygen boundary conditions are likely to be the same among the different alloys, and the different oxidation potential of precipitates cannot explain the observed variations in the δ_{met} threshold value [67]. Thus, at a given oxide thickness, the oxygen partial pressure in the Zr-2.5Nb oxide layer is lower than the oxygen partial pressure in ZIRLO, which is in turn lower than the oxygen partial pressure in Zircaloy-4 oxide layers. When the oxide transition occurs and the oxide is no longer protective and is permeable to water, so that δ_{met} drops to zero (Fe and Nb are fully oxidized).

It is thought that the development of porosity in the protective oxide layers is responsible for the fact that δ_{met} reaches a threshold. The evolution of the microporosity in zirconium oxide layers as a function of oxide thickness has been extensively studied [26,68–72] and the reported values of an oxide thickness free of

interconnected pores (0.8 μm to 1.2 μm) are in agreement with our reported values of δ_{met} as a function of δ_p. Before transition, the formation of a connected network of pores would increase the partial pressure of oxygen in the outer part of the protective oxide layer. Once the precipitates are embedded in the outer part of the oxide layer where pores are interconnected, they will oxidize. δ_{met} represents the boundary between the inner part of the oxide, free of interconnected pores, and the outer part in which pores are interconnected. It is of course tempting to relate δ_{met} to the concept of a barrier layer as defined by other authors [11], but it is necessary to carefully define the barrier layer concept, as different techniques will yield different values of δ_{met}.

Yilmazbayhan et al. have shown that for the same alloys used in this study, the higher the post-transition corrosion rate, the smaller the oxide thickness at transition [20]. The Zircaloy-4 transition being the earliest (and its corrosion rate the highest) among the alloys studied, its level of porosity at a given oxide thickness would be the highest among the considered alloys [71]. Different levels of porosity among the alloys (highest for Zircaloy-4 and lowest for Zr-2.5Nb) would explain the different threshold values of δ_{met} (smallest for Zircaloy-4 and highest for Zr-2.5Nb).

Effect of Precipitate Oxidation on Hydrogen Pickup Fraction

The ratio $\delta_{\text{met}}/\delta_p$ and the instantaneous hydrogen pickup fraction f_H^i are plotted in Fig. 11 as a function of δ_p for all the alloys (f_H^i is plotted in a similar fashion as in Fig. 8). The transition thickness for Zr-0.4Fe-0.2Cr (H) is unknown, and the third transition of Zircaloy-4 is not precisely known. The *total* hydrogen pickup fraction is plotted in the case of Zr-0.4Fe-0.2Cr (H). In Fig. 11(*b*), the pickup fraction at 0 μm is the total hydrogen pickup fraction from $t = 0$ days to the time at the first transition [Fig. 11(*c*) shows the same for the second transition].

It appears that variations in $\delta_{\text{met}}/\delta_p$ and f_H^i are connected. At first, the concentration of metallic precipitates in the protective oxide layer, represented by the ratio $\delta_{\text{met}}/\delta_p$, is constant, so that σ_e^{ox} is constant until δ_{met} reaches its threshold value. According to the hypothesis that hydrogen pickup results from the need to balance charge, f_H^i would remain constant as observed in Figs. 11(*b*) and 11(*d*). As explained in the preceding section, because of the development of microporosity in the outer part of the protective oxide layer, the ratio $\delta_{\text{met}}/\delta_p$ decreases and the concentration of metallic precipitates acting as local electric shortcuts in the oxide layer decreases. As a result, σ_e^{ox} would also decrease, and f_H^i would increase up to transition. This effect is observed in all the plots in Fig. 11. Eventually, the same mechanism will take place in the next transition period.

However, the observed increase in f_H from one transition period to the next cannot be fully explained by this mechanism, because the growth of the oxide layer and the oxidation of alloying elements are periodic processes. The likely explanation for this difference is that one of the boundary conditions is changing after transition. One possibility is that the presence of the outer porous oxide changes the

FIG. 11 Instantaneous hydrogen pickup fraction (at the bottom) and the ratio δ_{met}/δ_p of Fe and/or Nb (at the top) as a function of the protective oxide thickness δ_p (in micrometers) for various alloys and transition regimes: (a) Zircaloy-4 pre-transition (b) Zircaloy-4 in the transition period; (c) Zircaloy-4 before the second transition period; (d) ZIRLO; (e) Zr-2.5Nb; and (f) Zr-0.4Fe-0.2Cr (H). The shaded area shows the transition thickness for the different alloys (unknown for Zr-0.4Fe-0.2Cr (H) and Zircaloy-4 at the third transition). In the case of Zr-0.4Fe-0.2Cr (H), the total hydrogen pickup fraction is plotted instead of the instantaneous hydrogen pickup fraction.

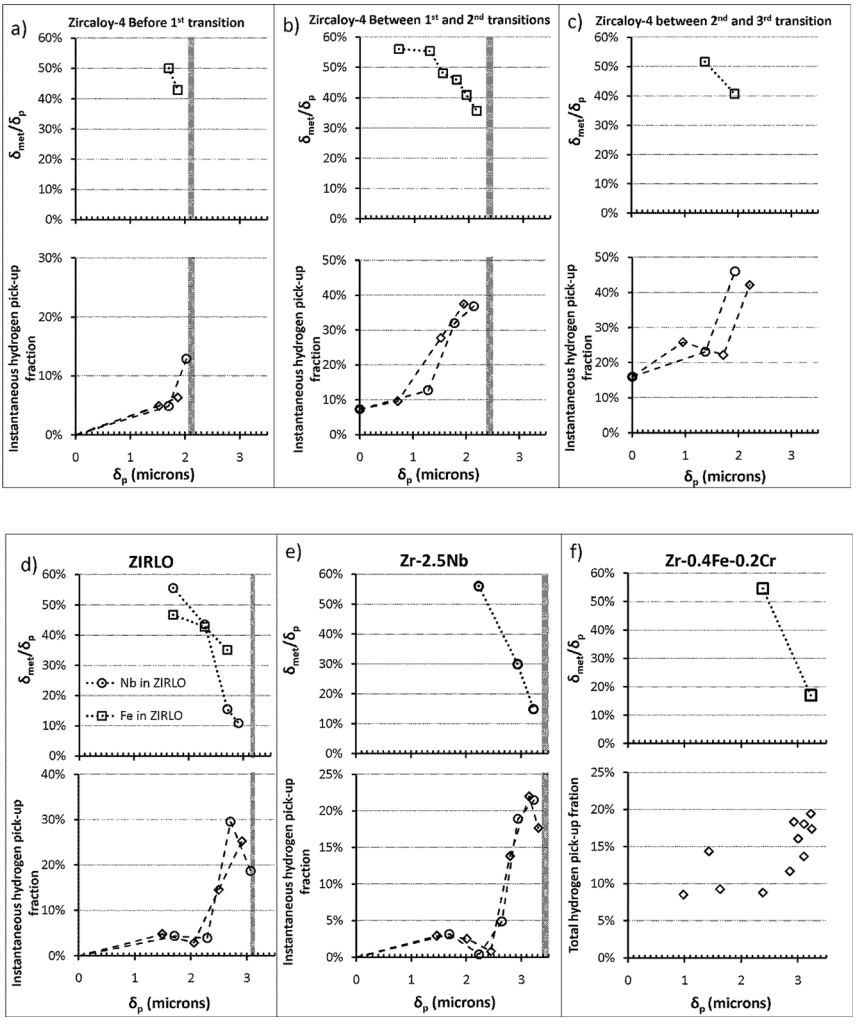

boundary condition at the outer limit of the protective oxide. Previous studies have indicated that hydrogen overpressure increases hydrogen pickup in zirconium alloys [10,73]. In the pre-transition regime, the cathodic site is directly in contact with water, so that the hydrogen pressure at the cathodic site and that in the water are equal. However, when a non-protective oxide layer is present on the top of the growing protective oxide, the hydrogen evolved at the cathodic site has to diffuse through these layers to finally reach the water. As a result, a hydrogen pressure gradient will be established across the non-protective oxide layers. This will cause hydrogen overpressure at the hydrogen evolution site to build up, leading to an increase in proton concentration at this location. Higher concentrations of protons at the interface could lead to an increase in hydrogen pickup fraction such as seen in Fig. 5.

Conclusion

Detailed measurements were performed for hydrogen pickup and oxide growth as a function of exposure time for a set of chosen zirconium alloys with specific chemistries and microstructures using vacuum hot extraction (VHE) and cold neutron prompt gamma activation analysis (CNPGAA). The variations of the oxidation states of Fe and Nb as a function of oxide depth in these samples were investigated by means of x-ray absorption near edge spectroscopy (XANES) using microbeam synchrotron radiation.

1. The hydrogen pickup fraction is linked to the corrosion kinetics but does not follow it exactly. Results are consistent with the hypothesis that the higher the oxide electronic conductivity, the higher the corrosion rate and the lower the pickup fraction. Hydrogen pickup during corrosion results from the need to balance charge, causing hydrogen pickup to increase when the rate of electron transport through the protective oxide decreases. According to this, oxide electronic conductivity ($\sigma_{e^-}^{ox}$) plays a key role in the hydrogen pickup mechanism, such that alloy oxides with higher $\sigma_{e^-}^{ox}$ result in a lower hydrogen pickup fraction, and vice versa.
2. Nb additions generally reduce the hydrogen pickup fraction. Following the previously stated hypothesis, it is proposed that the donor effect of Nb in solid solution increases $\sigma_{e^-}^{ox}$, thereby reducing hydrogen pickup. The oxidation of Fe and Nb when incorporated into the oxide is delayed relative to zirconium oxidation. Thus metallic precipitates are embedded in the growing oxide up to a thickness of δ_{met}. It is proposed that metallic precipitates embedded in the protective oxide reduce hydrogen pickup by increasing $\sigma_{e^-}^{ox}$, possibly by acting as local electric shortcuts.
3. An oxidation model of precipitates has been developed: an inner layer (thickness $= \delta_{met}$) in which most of the alloying elements in precipitates are still metallic develops as the oxide grows. At first δ_{met} increases as the protective oxide layer thickens. After the oxide layer grows up to a threshold value of around 1 μm to 1.5 μm, δ_{met} reaches a constant value that lasts until the oxide reaches transition, when δ_{met} drops to zero. This threshold value is alloy

dependent and has been connected to the development of microporosity in the oxide. The alloys scale as follows: the higher the corrosion rate, the higher the porosity and the lower the δ_{met}.

4. The evolution of δ_{met}/δ_p is connected to the evolution of the instantaneous hydrogen pickup fraction in all the studied alloys. The increase in instantaneous hydrogen pickup fraction as the corrosion rate slows down is rationalized to the delayed oxidation of precipitates in the protective oxide layer.

ACKNOWLEDGMENTS

The writers thank R. Paul at NIST for CNPGAA measurements and Z. Cai for his expert assistance in μXANES experiments at APS. This research was funded by EPRI and Westinghouse Electric Co. LLC. Usage of the Advanced Photon Source was supported by the U.S. Department of Energy, Office of Basic Energy Sciences, under Contract No. DE-AC02-06CH11357. The writers also thank the community of the MUZIC-2 program for support and helpful discussions. The writers thank K. Sakamoto from Nippon Nuclear Fuel Development and G. Kuri from Paul Scherrer Institute for helpful discussions. The writers thank Benoit de Gabory and Aditya Shivprasad for their assistance in performing the XANES experiments.

References

[1] "Corrosion of Zirconium Alloys in Nuclear Power Plants," *IAEA-TECDOC-684*, International Atomic Energy Agency, Vienna, 1993.

[2] "Waterside Corrosion of Zirconium Alloys in Nuclear Power Plants," *IAEA-TECDOC-996*, International Atomic Energy Agency, Vienna, 1998.

[3] Cox, B., "Some Thoughts on the Mechanisms of In-reactor Corrosion of Zirconium Alloys," *J. Nucl. Mater.*, Vol. 336, 2005, pp. 331–368.

[4] Kass, S., "Hydrogen Pickup in Various Zirconium Alloys during Corrosion Exposure in High-Temperature Water and Steam," *J. Electrochem. Soc.*, Vol. 107, 1960, pp. 594–597.

[5] Klepfer, H. H., "Hydrogen Uptake of Zirconium Alloys during Water and Steam Corrosion," *Corrosion*, Vol. 19, 1963, p. 285.

[6] Berry, W. E., Vaughan, D. A., and White, E. L., "Hydrogen Pickup During Corrosion of Zirconium Alloys", *Corrosion*, Vol. 17, 1961, p. 109.

[7] Cox, B., "A Mechanism for the Hydrogen Uptake Process in Zirconium Alloys," *J. Nucl. Mater.*, Vol. 264, 1999, pp. 283–294.

[8] Kass, S. and Kirk, W. W., "Corrosion and Hydrogen Absorption Properties of Nickel-free Zircaloy-2 and Zircaloy-4", *ASM Trans. Q.*, Vol. 55, 1962, pp. 77–100.

[9] Hatano, Y., Sugisaki, M., Kitano, K., and Hayashi, M., "Role of Intermetallic Precipitates in Hydrogen Transport through Oxide Films on Zircaloy," *Zirconium in the Nuclear Industry: 12th International Symposium, ASTM STP 1354*, ASTM International, Philadelphia, PA, 2000, pp. 901–917.

[10] Hillner, E., *Hydrogen Absorption in Zircaloy During Aqueous Corrosion, Effect of Environment*, WAPD-TM-411, AEC Research and Development, Pittsburgh, PA, 1964.

[11] Adamson, R., Garzarolli, F., Cox, B., Strasser, A., and Rudling, P., *Corrosion Mechanisms in Zirconium Alloys*, A.N.T. International, Sweden, 2007.

[12] Kakiuchi, K., Itagaki, N., Furuya, T., Miyazaki, A., Ishii, Y., Suzuki, S., Terai, T., and Yamawaki, M., "Effect of iron on hydrogen absorption properties of zirconium alloys", *J. Phys. Chem. Solids*, Vol. 66, 2005, pp. 308–311.

[13] Harada, M. and Wakamatsu, R., "The Effect of Hydrogen on the Transition Behavior of the Corrosion Rate of Zirconium Alloys," *Zirconium in the Nuclear Industry: 15th International Symposium, ASTM STP 1505*, ASTM International, West Conshohocken, PA, 2008, p. 384.

[14] Grandjean, A. and Serruys, Y., "Metal and Oxygen Mobilities During Zircaloy-4 Oxidation at High Temperature," *J. Nucl. Mater.*, Vol. 273, 1999, pp. 111–115.

[15] Cox, B. and Pemsler, J. P., "Diffusion of Oxygen in Growing Zirconia Films," *J. Nucl. Mater.*, Vol. 28, 1968, pp. 73–78.

[16] Lemaignan, C. and Motta, A. T., *Zirconium Alloys in Nuclear Applications*, B. R. T. Frost, Ed., Vol. 10B, Material Science and Technology Series, VCH, New-York, R. W. Cahn, P. Haasen and E. J. Kramer, Eds., 1994, pp. 1–51.

[17] Hauffe, K., *Oxidation of Metals*, Plenum Press, New York, 1965.

[18] Sabol, G. P. and Dalgaard, S. B., "The Origin of the Cubic Rate Law in Zirconium Alloy Oxidation," *J. Electrochem. Soc.*, Vol. 122, 1975, pp. 316–317.

[19] Porte, H. A., Schnizlein, J. G., Vogel, R. C., and Fischer, D. F., "Oxidation of Zirconium and Zirconium Alloys", *J. Electrochem. Soc.*, Vol. 107, 1960, pp. 506–515.

[20] Yilmazbayhan, A., Motta, A. T., Comstock, R. J., Sabol, G. P., Lai, B., and Cai, Z., "Structure of Zirconium Alloy Oxides Formed in Pure water Studied with Synchrotron Radiation and Optical Microscopy: Relation to Corrosion Rate," *J. Nucl. Mater.*, Vol. 324, 2004, pp. 6–22.

[21] Motta, A. T., Gomes Da Silva, M. J., Yilmazbayhan, A., Comstock, R. J., Cai, Z., and Lai, B., "Microstructural Characterization of Oxides Formed on Model Zr Alloys Using Synchrotron Radiation," *Zirconium in the Nuclear Industry: 15th International Symposium, ASTM STP 1505*, ASTM International, West Conshohocken, PA, 2009, p. 486.

[22] Bradhurst, D. H., Draley, J. E., and Van Drunen, C. J., "An Electrochemical Model for the Oxidation of Zirconium," *J. Electrochem. Soc.*, Vol. 112, 1965, pp. 1171–1177.

[23] Cox, B., "Rate Controlling Processes During the Pre-transition Oxidation of Zirconium Alloys", *J. Nucl. Mater.*, Vol. 31, 1969, pp. 48–66.

[24] Cox, B., *Rate Controlling Processes During the Oxidation of Zirconium Alloys*, AECL-2777, Atomic Energy of Canada Limited, Chalk River, ON, Canada, 1967.

[25] Frank, H., "Transport Properties of Zirconium Alloy Oxide Films", *J. Nucl. Mater.*, Vol. 306, 2002, pp. 85–98.

[26] Ramasubramanian, N., Billot, P., and Yagnik, S., "Hydrogen Evolution and Pickup During the Corrosion of Zirconium Alloys: A Critical Evaluation of the Solid State and Porous

Oxide Electrochemistry," *Zirconium in the Nuclear Industry: 13th International Symposium, ASTM STP 1423*, ASTM International, Philadelphia, PA, pp. 222–244, 2002.

[27] Beie, H.-J., Mitwalsky, A., Garzarolli, F., Ruhmann, H., and Sell, H. J., "Examinations of the Corrosion Mechanism of Zirconium Alloys," *Zirconium in the Nuclear Industry: 10th International Symposium, ASTM STP 1245*, ASTM International, Philadelphia, PA, 1994, pp. 615–643.

[28] Shirvington, P. J., "Electron Conduction Through Oxide Films on Zircaloy," *J. Nucl. Mater.*, Vol. 37, 1970, pp. 177–202.

[29] Howlader, M. M. R., Shiiyama, K., Kinoshita, C., Kutsuwada, M., and Inagaki, M., "The Electrical Conductivity of Zircaloy Oxide Films," *J. Nucl. Mater.*, Vol. 253, 1998, pp. 149–155.

[30] Hartman, T. E., Blair, J. C., and Bauer, R., "Electrical Conduction through SiO Films," *J. Appl. Phys.*, Vol. 37, 1966, pp. 2468–2474.

[31] Simmons, J. G., "Poole-Frenkel Effect and Schottky Effect in Metal-Insulator-Metal Systems," *Phys. Rev.*, Vol. 155, 1967, pp. 657–660.

[32] Ramasubramanian, N., "Localised Electron Transport in Growing Zirconium Alloys," *J. Nucl. Mater.*, Vol. 55, 1975, pp. 134–154.

[33] Baur, K., Garzarolli, F., Ruhmann, H., and Sell, H.-J., "Electrochemical Examinations in 350°C Water with Respect to the Mechanism of Corrosion-hydrogen Pickup," *Zirconium in the Nuclear Industry: 12th International Symposium, ASTM STP 1354*, ASTM International, West Conshohocken, PA, 2000, pp. 836–852.

[34] Gohr, H., Schaller, J., Ruhmann, H., and Garzarolli, F., "Long-term In Situ Corrosion Investigation of Zr Alloys in Simulated PWR Environment by Electrochemical Measurements," *Zirconium in the Nuclear Industry: 11th International Symposium, ASTM STP 1295*, ASTM International, West Conshohocken, PA, 1996, pp. 181–202.

[35] Harding, J. H., "The effect of alloying elements on Zircaloy corrosion", *J. Nucl. Mater.*, Vol. 202, 1993, pp. 216–221.

[36] Taylor, D. F., "An Oxide-semiconductance Model of Nodular Corrosion and its Application to Zirconium Alloy Development", *J. Nucl. Mater.*, Vol. 184, 1991, pp. 65–77.

[37] Urquhart, A. W., Vermilyea, D. A., and Rocco, W. A., "Mechanism for the Effect of Heat-Treatment on the Accelerated Corrosion of Zircaloy-4 in High Temperature, High Pressure Steam," *J. Electrochem. Soc.*, Vol. 125, 1978, pp. 199–204.

[38] Smith, T., "Kinetics and Mechanism of Hydrogen Permeation of Oxide Films on Zirconium," *J. Nucl. Mater.*, Vol. 18, 1966, pp. 323–336.

[39] Malki, B., Le Bacq, O., and Pasturel, A., "Ab initio Study of Hydrogen Related Defect in ZrO2: Consequences on Dry and Aqueous Oxidation," *J. Nucl. Mater.*, Vol. 416, 2011, pp. 362–368.

[40] Draley, J. E. and Ruther, W. E., "Some Unusual Effects of Hydrogen in Corrosion Reactions," *J. Electrochem. Soc.*, Vol. 104, 1957, pp. 329–333.

[41] Kiselev, A. A., *Research on the Corrosion of Zirconium Alloys in Water and Steam at High Temperature and Pressure*, AECL-1724, Atomic Energy of Canada Limited, Chalk River, Ontario, CA 1963.

[42] Choo, K.-N., Pyun, S.-I., and Kim, Y.-S., "Oxidation and Hydrogen Uptake of Zr Based Nb Alloys at 400°C Under 10 MPa H_20 Steam Atmosphere", *J. Nucl. Mater.*, Vol. 226, 1995, pp. 9–14.

[43] McIntyre, N. S., Davidson, R. D., Weisener, C. G., Good, G. M., Mount, G. R., Warr, B. D., and Elmoselhi, M., "Migration of hydrogen through thin films of ZrO_2 on Zr-Nb alloy" *J. Vac. Sci. Technol. A*, Vol. 9, 1991, pp. 1402–1405.

[44] Bossis, P., Pecheur, D., Hanifi, K., Thomazet, J., and Blat, M., "Comparison of the High Burn-up Corrosion on M5 and Low Tin Zircaloy-4," *Zirconium in the Nuclear Industry: 14th International Symposium, ASTM STP 1467*, ASTM International, West Conshohocken, PA, 2005, pp. 494–524.

[45] Cox, B., "Hydrogen Absorption by Zircaloy-2 and Some Other Alloys during Corrosion in Steam", *J. Electrochem. Soc.*, Vol. 109, 1962, pp. 6–12.

[46] Couet, A., Motta, A. T., and Comstock, R. J., "Hydrogen Pickup Measurements in Zirconium Alloys: Relation to Corrosion Rate," *J. Nucl. Mater.* (submitted).

[47] Gomes Da Silva, M. J., 2007, "Influence of Oxide Microstructure on Corrosion Behavior of Zirconium-based Model Alloys," Ph.D. thesis in Nuclear Engineering, Penn State University, University Park, PA.

[48] ASTM G2/G2M-06: Standard Test Method for Corrosion Testing of Products of Zirconium, Hafnium, and Their Alloys in Water at 680°F or in Steam at 750°F, *Annual Book of ASTM Standards*, ASTM International, West Conshohocken, PA, 2011.

[49] ASTM E146-83: Methods of Chemical Analysis of Zirconium and Zirconium Alloys (Silicon, Hydrogen, and Copper), *Annual Book of ASTM Standards*, ASTM International, West Conshohocken, PA, 1989.

[50] Couet, A., Motta, A. T., Comstock, R. J., and Paul, R. L., "Cold Neutron Prompt Gamma Activation Analysis, a Non-destructive Technique for Hydrogen Level Assessment in Zirconium Alloys," *J. Nucl. Mater.*, Vol. 425, 2012, pp. 211–217.

[51] Wiese, H., 1999, "Fractionated Determination of Hydrogen in Corroded Zirconium Alloys," Ph.D. thesis, Paul Scherrer Institute, Villigen.

[52] Couet, A., Motta, A. T., De Gabory, B., and Cai, Z., "X-ray Absorption Near-edge Spectroscopy Study of Fe and Nb Oxidation States Evolution in Zircaloy-4, ZIRLO, Zr-2.5Nb and Zr-0.4Fe-0.2Cr Oxide Layers," *J. Nucl. Mater.* (submitted).

[53] Ravel, B. and Newville, M., "Athena, Arthemis, Hephaestus: Data Analysis for X-Ray Absorption Spectroscopy Using IFEFFIT," *J. Synchrotron Radiat.*, Vol. 12, 2005, pp. 537–541.

[54] Henke, B. L., Gullikson, E. M., and Davis, J. C., *At. Data Nucl. Data Tables*, Vol. 54, 1993, pp. 181–342.

[55] Charquet, D., Hahn, R., Ortlieb, E., Gros, J.-P., and Wadier, J.-F., "Solubility Limits and Formation of Intermetallic Precipitates in ZrSnFeCr Alloys," *Zirconium in the Nuclear Industry: 8th Symposium, ASTM STP 1023*, ASTM International, West Conshohocken, PA, 1988, pp. 405–422.

[56] Yilmazbayhan, A., Delaire, O., Motta, A. T., Birtcher, R. C., Maser, J. M., and Lai, B., "Determination of the alloying content in the matrix of Zr alloys using synchrotron radiation microprobe X-ray fluorescence", *J. Nucl. Mater.*, Vol. 321, 2003, pp. 221–232.

[57] Sakamoto, K., Une, K., and Aomi, M., "Chemical State of Alloying Elements in Oxide Layer of Zr-based Alloys," *ANS LWR Fuel Performance/Top Fuel/WRFPM*, Orlando, FL, Sept 26–29, 2010.

[58] Sakamoto, K., Une, K., Aomi, M., and Hashizume, K., "Depth Profile of Chemical States of Alloying Elements in Oxide Layer of Zr-based Alloys" *Prog. Nucl. Energy*, Vol. 57, 2012, pp. 101–105.

[59] Murai, T., Isobe, K., Takizawa, Y., and Mae, Y., "Fundamental Study on the Corrosion Mechanism of Zr-0.2Fe, Zr-0.2Cr and Zr-0.1Fe-0.2Cr Alloys," *Zirconium in the Nuclear Industry: 12th International Symposium, ASTM STP 1354*, ASTM International, West Conshohocken, PA, 2000, pp. 623–640.

[60] Broy, Y., Garzarolli, F., Seibold, A., and Van Swam, L. F., "Influence of Transition Elements Fe, Cr, and V on Long-time Corrosion in PWRs," *Zirconium in the Nuclear Industry: 12th International Symposium, ASTM STP 1354*, ASTM International, West Conshohocken, PA, 2000, pp. 609–622.

[61] Abriata, J. P. and Bolcich, J. C., "The Zr-Nb (Zirconium-Niobium) System," *Bull. Alloy Phase Diagrams*, Vol. 3, 1982, pp. 1710–1712.

[62] Froideval, A., Abolhassani, S., Gavillet, D., Grolimund, D., Borca, C., Krbanjevic, J., and Degueldre, C., "Microprobe Analysis of Neutron Irradiated and Autoclaved Zirconium Niobium Claddings Using Synchrotron-based Hard X-ray Imaging and Imaging," *J. Nucl. Mater.*, Vol. 385, 2009, pp. 346–350.

[63] Kim, B.-Y., Park, C.-J., and Kwon, H.-S., "Effect of Niobium on the Electronic Properties of Passive Films on Zirconium Alloys," *J. Electroanal. Chem.*, Vol. 576, 2005, pp. 269–276.

[64] Pêcheur, D., "Oxidation of Beta-Nb and $Zr(Fe,V)_2$ Precipitates in Oxide Films Formed on Advanced Zr-based Alloys," *J. Nucl. Mater.*, Vol. 278, 2000, pp. 195–201.

[65] Pêcheur, D., Lefebvre, F., Motta, A. T., Lemaignan, C., and Wadier, J. F., "Precipitate Evolution in the Zircaloy-4 Oxide Layer," *J. Nucl. Mater.*, Vol. 189, 1992, pp. 318–332.

[66] Barberis, P., Ahlberg, E., Simic, N., Charquet, D., Dahlback, M., Limback, M., Tagstrom, P., Lemaignan, C., Wikmark, G., and Lehtinen, B., "Role of Second Phase Particles in Binary Zirconium Alloys," *Zirconium in the Nuclear Industry: 13th International Symposium, ASTM STP 1423*, ASTM International, West Conshohocken, PA, 2001, pp. 33–58.

[67] Proff, C., Abolhassani, S., and Lemaignan, C., "Oxidation Behaviour of Zirconium Alloys and Their Precipitates — A Mechanistic Study," *J. Nucl. Mater.*, Vol. 432, 2013, pp. 222–238.

[68] Bossis, P., Lelievre, G., Barberis, P., Iltis, X., and Lefebvre, F., "Multi-scale Characterization of the Metal-Oxide Interface of Zirconium Alloys," *Zirconium in the Nuclear Industry: 12th International Symposium, ASTM STP 1354*, ASTM International, West Conshohocken, PA, 2000, pp. 918–947.

[69] Cox, B., "Pore Structure in Oxide Films Irradiated and Unirradiated Zirconium Alloys," *J. Nucl. Mater.*, Vol. 148, 1987, pp. 332–343.

[70] Ploc, R. A. and Newcomb, S. B., "Porosity in Zr-2.5Nb Corrosion Films," *Microscopy of Oxidation 3: Proceedings of the Third International Conference on the Microscopy of Oxidation*, Cambridge, UK, Sept 16–18, 1996, pp. 475–487.

[71] Ni, N., Lozano-Perez, S., Jenkins, M. L., English, C., Smith, G. D. W., Sykes, J. M., and Grovenor, C. R. M., "Porosity in Oxides on Zirconium Fuel Cladding Alloys, and its Importance in Controlling Oxidation Rates", *Scr. Mater.*, Vol. 62, 2010, pp. 564–567.

[72] Une, K., Sakamoto, K., Aomi, M., Matsunaga, J., Etoh, Y., Takagi, I., Miyamura, S., Kobayashi, T., and Ito, K., "Hydrogen Absorption Mechanism of Zirconium Alloys Based on Characterization of Oxide Layer," *Zirconium in the Nuclear Industry: 16th International Industry, ASTM STP 1529*, ASTM International, West Conshohocken, PA, 2011, pp. 401–432.

[73] Cox, B., "Assessment of In-Reactor Corrosion Models and Data for Zircaloys in Water," *2nd International Symposium on Environmental Degradation of Materials in Nuclear Power Systems—Water Reactors*, Monterey, CA, Sept 9–12, 1985, pp. 219–226.

DISCUSSION

Questions from N. Ramasubramanian, ECCATEC Inc. Canada

Q1:—How does the differential hydrogen pickup fraction vary with weight gain?

Authors' Response:—The differential hydrogen pickup fraction is defined as the instantaneous hydrogen pickup fraction f_H^i, which is equal to:

$$f_H^i = \frac{\frac{dH_{absorbed}}{dt}}{\frac{dH_{generated}}{dt}} \sim \lim_{\Delta\tau \to 0} \frac{\Delta_t^{t+\Delta t} H_{absorbed}}{\Delta_t^{t+\Delta t} H_{generated}} \propto \frac{dH_{absorbed}}{d\delta}$$

Variations of this derivative as function of exposure time can be observed in Figure 8 on ZIRLO. On the same figure, weight gain is plotted so that we can have a general idea of how f_H^i behaves as a function of weight gain w_g. To have a better description of this dependence, in the following figure we plotted the fit of f_H^i as function of the fit of weight for ZIRLO (the fits details are provided in [1])

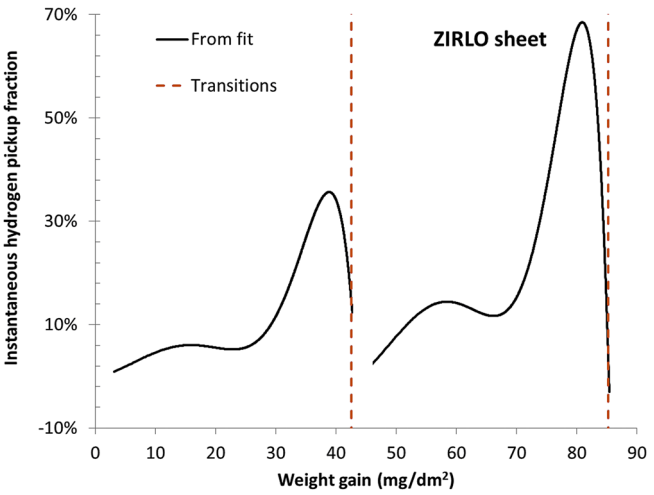

Instantaneous hydrogen pickup fraction as function of oxide thickness (or weight gain) follows a general trend common to every alloy studied in this paper:

- At small protective oxide thickness (<40% of oxide thickness at transition), f_H^i increases with oxide thickness.
- Between 40% and 70% of oxide thickness at transition, f_H^i reaches a plateau.
- Above 70% of oxide thickness at transition, f_H^i starts to steadily increase again, reaching a peak and decrease right before oxide transition.

Q2:—Does hydrogen evolution, assisted by electron transport via segregated iron, occur at the oxide coolant interface?

Authors' Response:—It is believed that the hydrogen evolution reaction leading to the formation of hydrogen gas occurs at the oxide/coolant interface. However, some hydrogen from the corrosion reaction enters the oxide under the form of protons and recombine either in the oxide or at the metal/oxide interface and not at the oxide/coolant interface. The location of these cathodic sites inside the oxide and the fate of hydrogen evolved in the oxide are not known at the moment.

Q3:—Protectiveness and pickup fraction: the more protective the oxide, the higher the pickup fraction? Does this mean protective for electron transport (insulating)?

Authors' Response:—Indeed, the conclusions of our study seem to show this correlation: the more insulating the oxide is, the higher the hydrogen pickup fraction since the transport of electrons is more difficult. The difficulty of electron transport is transcribed as a higher electric potential across the oxide, believed to be the driving force for protons to get into the oxide. By adding a donor such as Nb^{5+} and/or metallic second phase particles in the insulating oxide, the insulating oxide could be more conductive for electrons, lowering the electrical potential across the oxide, so that the driving force for hydrogen pickup would be reduced.

Question from B. K. Shah, BARC Mumbai

Q1:—Does Cold Neutron Prompt Gamma Activation Analysis for non-destructive measurement of hydrogen in Zr alloys measure hydrogen in the surface layer or is it a bulk analysis? What is the uncertainty in hydrogen measurement by this method?

Authors' Response:—This method measures the hydrogen concentration in the whole thickness of the sample as long as the sample is not too thick (not thicker than 1 cm or so). Indeed if it is too thick, neutron beam energy would vary inside of the sample due to neutron thermalization and thus the reaction rate between hydrogen and neutrons would change as function of sample depth, leading to erroneous hydrogen concentrations. Correction factors need to be precisely determined before proceeding on thick samples. The beam size is approximately 2 cm in diameter. Thus an average bulk concentration of hydrogen is obtained in the region where the beam covers the sample [2].

The uncertainty depends on many parameters (geometry at the beamline, signal to noise ratio and fitting procedure of the results) but was on the order of 5wt.ppm at the maximum in our study [2–4].

Q2:—What is the effect of Fe impurity in Zr-2.5Nb alloy on hydrogen pickup?

Authors' Response:—See response to J.-C. Brachet in the following.

Question from S. K. Jha, Nuclear Fuel Complex, Hyderabad:—What is the effect of Fe in Zr-2.5Nb as far as hydrogen pickup is concerned?

Authors' Response:—See response to J.-C. Brachet in the following.

Question from J. -C. Brachet, CEA Saclay, Nuclear Materials Dept. France:—The presentation from D. Kaczorowski showed no significant effects of Fe content on hydrogen pickup of M5 from ∼200 wt.ppm up to ∼1000 wt.ppm, suggesting a factor of approximately five between the ZrNbFe volumetric fractions. How do you explain this?

Authors' Response:—The conclusions of the study show that oxidations of Nb and/or Fe in precipitates (either $Zr(Fe,Cr)_2$, ZrNb or ZrNbFe) are delayed. Both elements are incorporated in a metallic state in the oxide layer (either in the form of precipitates as shown in the present paper or in solid solution in the case of Fe [5]) and their delayed oxidations are correlated to the increase in instantaneous hydrogen pickup fraction (see Figure 11). The f_H^i evolution is similar for every alloy, thus, not the type of precipitates but rather their delayed oxidation (observed on every studied alloys) has an impact on the increase in instantaneous hydrogen pickup fraction.

We did not perform XANES on Fe impurity in Zr-2.5Nb. However it is believed that Fe as an impurity in Zr-2.5Nb has little effect on hydrogen pickup, its effect being screened by the dopant effect of Nb saturated in solid solution and the metallic ZrNb precipitates. If there is sufficient Nb in solid solution, the Fe content as an impurity (several hundreds of wt.ppm) would not play a significant role in the hydrogen pickup mechanism in autoclave conditions. This is why it is mainly in its solid solution range that Nb concentration has an effect on electronic conductivity [6] and hydrogen pickup [7]. D. Kaczorowski's paper included in these proceedings confirms that Fe concentration up to 1000 wt.ppm in M5 (∼Zr-1.0Nb) has no noticeable effect on corrosion and hydrogen pickup. A thorough study of the electronic levels of metallic/oxidized isolated elements and clusters in the zirconium oxide band gap would be necessary to assess their effect on electronic transport.

Question from S. Ortner, Nuclear National Laboratories, U.K.:—Please clarify the range of time over which δ_{met} is increasing so we can compare with the time over which the instantaneous hydrogen pickup fraction f_H^i is shown to be approximately constant, increasing or decreasing.

Authors' Response:—Since the range of time, $\delta_{me\tau}$, and f_H^i are upon the alloy dependent, let us consider the alloy for which we have the most experimental data: Zircaloy-4.

Up to $\delta_p \sim 1.3\ \mu$m ($\sim$19 days of exposure time), $\delta_{me\tau}$ increases up to $\sim 0.8\ \mu$m (see Figure 9.a). In that range of time, $\delta_{me\tau}$ increases linearly with δ_p meaning that the fraction of metallic particles in the oxide layer is constant ($\frac{\delta_{me\tau}}{\delta_p}$ is constant as seen in Figure 11.e). During the same period of time f_H^i is also approximately constant (see Figures 11).

From $\delta_p \sim 1.3\ \mu$m to transition at $f_H^i \sim 2.2\ \mu$m (from $\sim$19 days to $\sim$85 days of exposure time), $\delta_{me\tau}$ is constant ($\sim 0.8\ \mu$m for Zircaloy-4) but δ_p keeps on increasing. Thus the ratio $\frac{\delta_{me\tau}}{\delta_p}$ decreases meaning that the fraction of metallic particles in the oxide layer is decreasing. At the same time, f_H^i increases sharply as observed in Figures 11.

Eventually, the alloy reaches transition and $\delta_{me\tau}$ drops to zero. Even though this is not seen on Zircaloy-4 since the time range in which $\delta_{me\tau}$ drops to zero is extremely short (the alloy undergoes a sudden transition, confirmed by the weight gain data in Figure 4.b), the decrease in $\delta_{me\tau}$ before transition appears in the other alloys in Figure 9. Eventually the process repeats itself in the next transition regime because the oxidation kinetics and hydrogen pickup kinetics are periodic.

Question from M. Griffiths, AECL:—You showed results for the copper-containing alloy with high pickup fraction and low corrosion kinetics compared with all other Fe containing alloys. What can you say about any other differences in the microstructure (precipitate distribution in particular) that could affect the behavior?

Authors' Response:—SEM and TEM microscopy on Zr-2.5Nb-0.5Cu tube alloy have been performed. Synchrotron X-ray diffraction experiments have also been performed on that alloy and β-Nb, C14 $Zr(Nb,Fe)_2$ and $Zr(Nb,Cu)_2$ Laves phase and tetragonal Zr_2Cu phases have been detected [8]. Using scanning TEM and SEM, Cu precipitates were characterized. Their sizes vary between 0.2 to 1 μm. They are elongated along the rolling direction (parallel to oxide/metal interface) and homogeneously distributed on the cross-section plane. The precipitate diameter in a Zr-0.5Cu binary alloy has been determined by synchrotron X-ray diffraction experiments and is on the order of 200 nm.

[1] A. Couet, *et al.*, "Hydrogen Pickup Measurements in Zirconium Alloys: Relation to Oxidation Kinetics," *Journal of Nuclear Materials*, accepted.

[2] A. Couet, *et al.*, "Cold neutron prompt gamma activation analysis, a non-destructive technique for hydrogen level assessment in zirconium alloys," *Journal of Nuclear Materials*, vol. 425, pp. 211–217, 2012.

[3] E. A. Mackey, *et al.*, "Sources of uncertainties in prompt gamma activation analysis," *Journal of Radioanalytical and Nuclear Chemistry*, vol. 265, pp. 273–281, 2005.

[4] R. Paul, "Hydrogen Measurement by Prompt Gamma-ray Activation Analysis: A Review," *Analyst*, vol. 122, pp. 35R–41R, 1997.

[5] A. Couet, *et al.*, "Title," unpublished.

[6] P. Chan-Jin, *et al.*, "Effect of niobium on the electronic properties of passive films on zirconium alloys," *Journal of Electroanalytical Chemistry*, vol. 576, pp. 269–76, 2005.

[7] A. A. Kiselev, "Research on the Corrosion of Zirconium Alloys in Water and Steam at High Temperature and Pressure," Atomic Energy of Canada Limited1963.

[8] A. T. Motta, *et al.*, "Microstructural Characterization of Oxides Formed on Model Zr Alloys Using Synchrotron Radiation," in *Zirconium in the Nuclear Industry: 15th International Symposium*, 2009, p. 486.